

2

# SRI International

**AD-A248 726**



Quarterly Technical Report 1 • February 1992

## FIELD-EMITTER ARRAYS FOR RF VACUUM MICROELECTRONICS

C.A. Spindt, Program Director  
A. Rosengreen, Senior Research Engineer  
Physical Electronics Laboratory

SRI Project 2743

Prepared for:

Defense Advanced Research Projects Agency  
Defense Sciences Office  
Virginia Square Plaza  
3701 North Fairfax Drive  
Arlington, VA 22203-1714

Attn: Dr. Bertram H. Hui

ARPA Order No. 8162

Contract MDA 972-91-C-0029

DTIC  
ELECTE  
APR 20 1992  
S C D

**92-09936**



The views and conclusions contained in this document are those of the authors and should not be interpreted as representing the official policies, either expressed or implied, of the Defense Advanced Research Projects Agency or the U.S. Government.

92 4 17 090

92 09 12

Approved for public release.  
Distribution unlimited

# FIELD-EMITTER ARRAYS FOR RF VACUUM MICROELECTRONICS

C.A. Spindt, Program Director  
A. Rosengreen, Senior Research Engineer  
Physical Electronics Laboratory

SRI Project 2743

Prepared for:

Defense Advanced Research Projects Agency  
Defense Sciences Office  
Virginia Square Plaza  
3701 North Fairfax Drive  
Arlington, VA 22203-1714

Attn: Dr. Bertram H. Hui

ARPA Order No. 8162

Contract MDA 972-91-C-0029

Accession For	
NTIS GRA&I	<input checked="" type="checkbox"/>
DTIC TAB	<input type="checkbox"/>
Unannounced	<input type="checkbox"/>
Justification:	
By:	
Distribution/	
Availability Codes	
Dist	Avail and/or Special
A-1	



The views and conclusions contained in this document are those of the authors and should not be interpreted as representing the official policies, either expressed or implied, of the Defense Advanced Research Projects Agency or the U.S. Government.

Approved:

Ivor Brodie, Director  
Physical Electronics Laboratory

Donald L. Nielson, Vice President  
Computing and Engineering Sciences Division

## SUMMARY

This report covers the first quarter of Phase I of a research and development program on the SRI Spindt-type field-emitter-array cathode with a view toward eventual applications in microwave amplifiers. Goals for this first phase have been set at 5 mA total emission with a current density of 5 A/cm<sup>2</sup> for at least 1 h and demonstrated modulation of the emission current at a frequency of 1 GHz. Our approach has been to identify methods of adapting and modifying the basic cathode structure for microwave operation and to experimentally investigate means of implementing those methods.

Two development areas required immediate attention. The first was to find a suitable material and then develop an anode that can be used in close proximity to the cathode without causing difficulties due to outgassing and arcing. The second was to design and fabricate a cathode structure with an interelectrode capacitance consistent with the microwave applications envisioned. In addition, work has begun on improving emitter-tip geometry and packing density with a view toward minimizing driving voltage requirements. Finally, we have started development of a test vehicle for characterizing the cathodes at microwave frequencies. The microwave measurements will be made using a Hewlett-Packard 8510B network analyzer.

The plan has been to research these issues in parallel. The cathode characterization and anode materials (and processing) issues were studied using our well-established cathode arrays fabricated on silicon substrates. Easy-to-build, low-frequency, triode configurations fabricated on standard TO-5 headers were used as the test vehicles. The low-capacitance cathode structure for high-frequency work is being studied using small-area cathode structures formed on dielectric (fused quartz) substrates, and a microwave test vehicle is being designed and built.

The results to date have been that 1000-tip arrays made in our traditional way on silicon substrates have been operated with a carefully processed close-spaced nickel anode ( $\approx 500 \mu\text{m}$  from the cathode) at 15 mA peak emission (15  $\mu\text{A}$  average peak current per tip) using a 60-Hz driver with a peak amplitude of 80 V for over 1000 h and continuing. (The duty cycle is 20%.) The arrays cover a  $256 \times 256\text{-}\mu\text{m}$  area, giving a peak current density of 22.8 A/cm<sup>2</sup>. The voltage on the anode is 180 V. These results demonstrate that the anode materials and processing selected for this test were well suited to the task.

Low-capacitance cathode arrays have been fabricated on glass substrates, and although there have been difficulties with a chemical vapor deposition (CVD) process used to form the oxide dielectric layer, low-capacitance cathodes have been fabricated and operated with encouraging results. The vendor doing the CVD service for us while our equipment is being brought on-line is confident that the problems (poor adhesion and cracking) can be overcome. In spite of the difficulty with the dielectric layer, some low-capacitance cathodes were tested and, in one case, 25-mA square-wave pulsed emission was obtained from a 625-tip array covering an area  $2.5 \times 10^{-5} \text{ cm}^2$  (1000 A/cm<sup>2</sup>). The pulse width was 5 ms and the duty cycle was 5%. The cathode emission was modulated at 20 MHz during the 5-ms pulse.

A test vehicle has been designed with 450°C-bakeable, ultra-vacuum-compatible, 50-ohm cables, microstrip lines, and connectors for operation at 1 GHz and higher, and construction will begin early in the next quarter.

## CONTENTS

<b>1. INTRODUCTION .....</b>	<b>1</b>
<b>2. EXPERIMENTAL CATHODE STRUCTURE.....</b>	<b>1</b>
<b>3. LOW-CAPACITANCE CATHODE FABRICATION.....</b>	<b>5</b>
<b>4. CATHODE EMISSION TESTS .....</b>	<b>10</b>
4.1 Close-Spaced Anodes.....	10
4.2 Low-voltage Cathode Geometry .....	13
4.3 Emission Tests with Low-Capacitance Cathodes .....	14
<b>5. MICROWAVE MEASUREMENTS.....</b>	<b>17</b>
<b>6. WORK PLANNED .....</b>	<b>19</b>
<b>REFERENCES .....</b>	<b>19</b>

## FIGURES

1	The SRI Spindt-type field-emission cathode array .....	2
2	Emitter strip (not to scale) .....	3
3	Top view of emitter strip in Figure 2 on a quartz substrate .....	3
4	Top view of emitter substrate bonded to two 50-ohm microstrip lines of which one supports the anode .....	4
5	Cross-sectional view of the structure in Figure 4 seen from the bottom up .....	5
6	Layout of the high-frequency test apparatus with sites for four cathodes .....	6
7	Detailed low-capacitance cathode layout .....	7
8	SEM and cross-section of a portion of a low-capacitance cathode structure with the dielectric layer undercut so that the gate film lifted and broke away from a large area .....	9
9	Schematic cross-sections of the close-spaced integrated nickel-plate anode and the stainless-steel tube anode .....	11
10	Emission data for 53i-300-8Q and 53i-300-8T (1000 emitter tips) .....	12
11	Cathode 53i-300-7P as fabricated and after 5 months (3600 h) of operation (1000 emitter tips) .....	14
12	Emission data for 1000-tip cathodes 53i-300-25B (average tips) and 53i-300-26B (tall, sharp tips) .....	15
13	Oscillographs of cathode 100L-A5-1A at 25 mA emission ( $1000 \text{ A/cm}^2$ ) with a 6 V peak-to-peak modulation voltage on the gate electrode .....	16
14	Current vs. $1/\text{voltage}$ plot for cathode 100L-A5-1A up to $1000 \text{ A/cm}^2$ .....	17

## 1. INTRODUCTION

The basic structure for the electron field-emitter array is the Spindt cathode shown in Figure 1. While this particular configuration is ideal for many applications, such as display devices, it is not suitable for use as a microwave device. The capacitance of the structure shown is much too large for driving the cathode at frequencies over a few hundred kilohertz.

The general expression for the cut-off frequency ( $f_t$ ) is given by  $f_t = g_m/2\pi C_g$  where  $g_m$  is the transconductance and  $C_g$  is the capacitance formed by the overlap of the gate and base (emitter) electrodes. To increase  $f_t$ , we must reduce the capacitance due to this overlap area and increase  $g_m$  by increasing the emitter tip density. (It is also possible to increase  $g_m$  somewhat by decreasing the operating voltage requirements.)

Figure 2 shows a sketch of a low-capacitance, high-tip-density structure that will be the basic configuration for this development program. The overlap (and therefore the capacitance) of the gate and base electrodes has been kept to a minimum by using a single row of emitters. A further decrease of the capacitance may be possible by removing most or all of the  $\text{SiO}_2$  layer in the overlap region, thereby reducing the dielectric constant from about 3.8 to about 1.0.

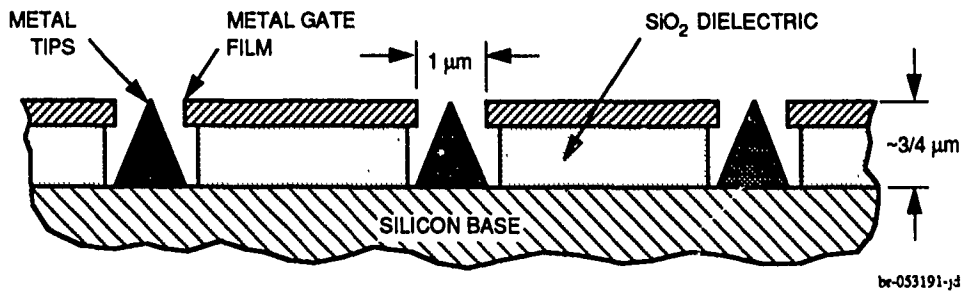
We will construct a simple triode for evaluating the microwave capabilities of such a gated cathode by adding an anode mounted on a separate substrate and positioned approximately a millimeter above the row of emitter tips. The triode structure will be characterized by measuring the scattering parameters (S-parameters) of the device using a Hewlett-Packard 8510B network analyzer. These parameters will then be used to evaluate the potential of the cathode as a microwave amplifier and to provide guidance for optimizing the device's performance.

Details of the experimental cathode, its fabrication, and evaluation procedures will be discussed in the following sections.

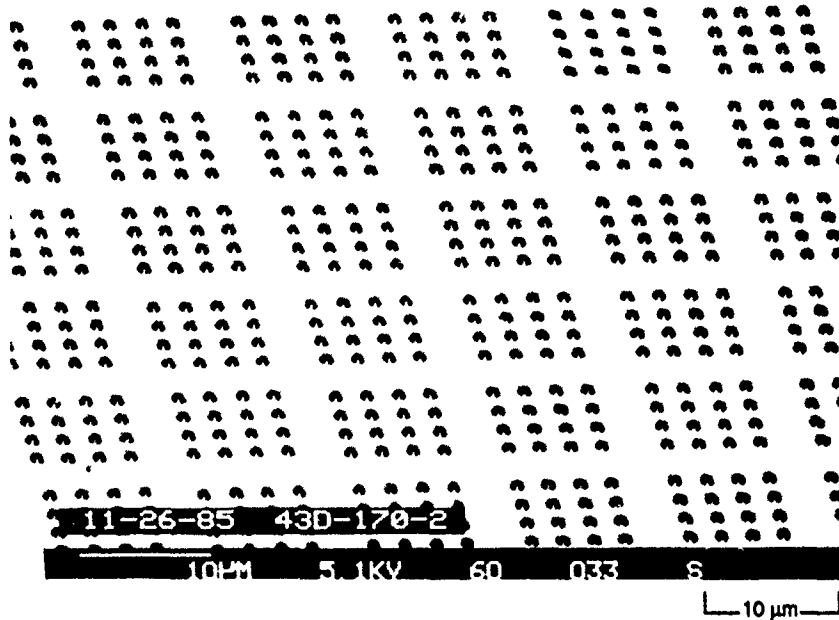
## 2. EXPERIMENTAL CATHODE STRUCTURE

Figure 3 shows a plan view of an emitter strip of the kind shown in Figure 2. The structure will be formed on a square, glass substrate approximately  $2.5 \times 2.5$  mm with a thickness of 0.65 mm. The row of emitters will be 1.25 mm long. The base and gate films will be kept as short as possible (within the constraints of the need to make reliable bonds to the microstrip lines) to minimize parasitic circuit elements.

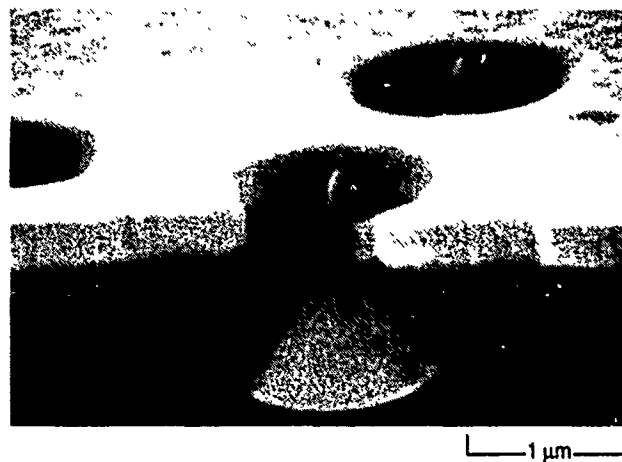
Figure 4 shows a plan view of the complete triode structure with the base electrode bonded to ground, and the gate and anode bonded to 50-ohm microstrip lines. The anode extends across the emitter chip approximately a millimeter above and slightly to the side of the



(a) SCHEMATIC OF A SPINDT CATHODE ARRAY

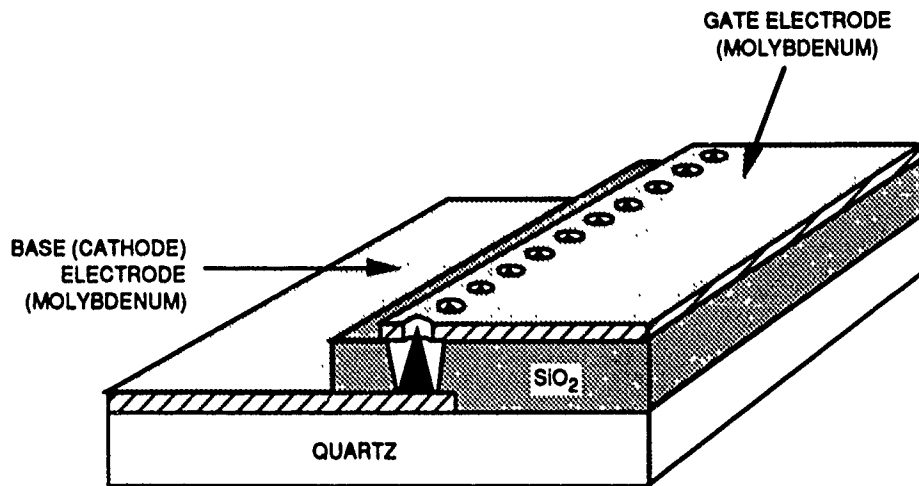


(b) SEM MICROGRAPH OF SPINDT CATHODE ARRAY



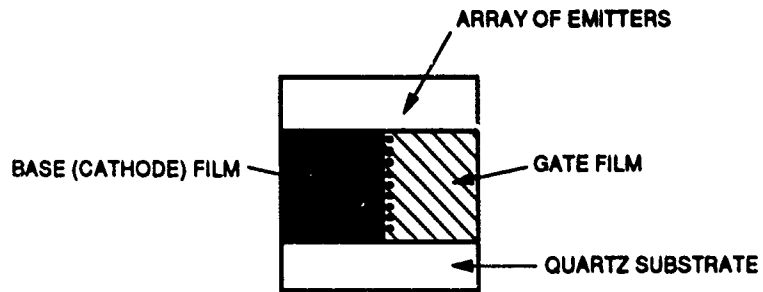
(c) SEM MICROGRAPH OF SPINDT CATHODE

Figure 1. The SRI Spindt-type field-emission cathode array



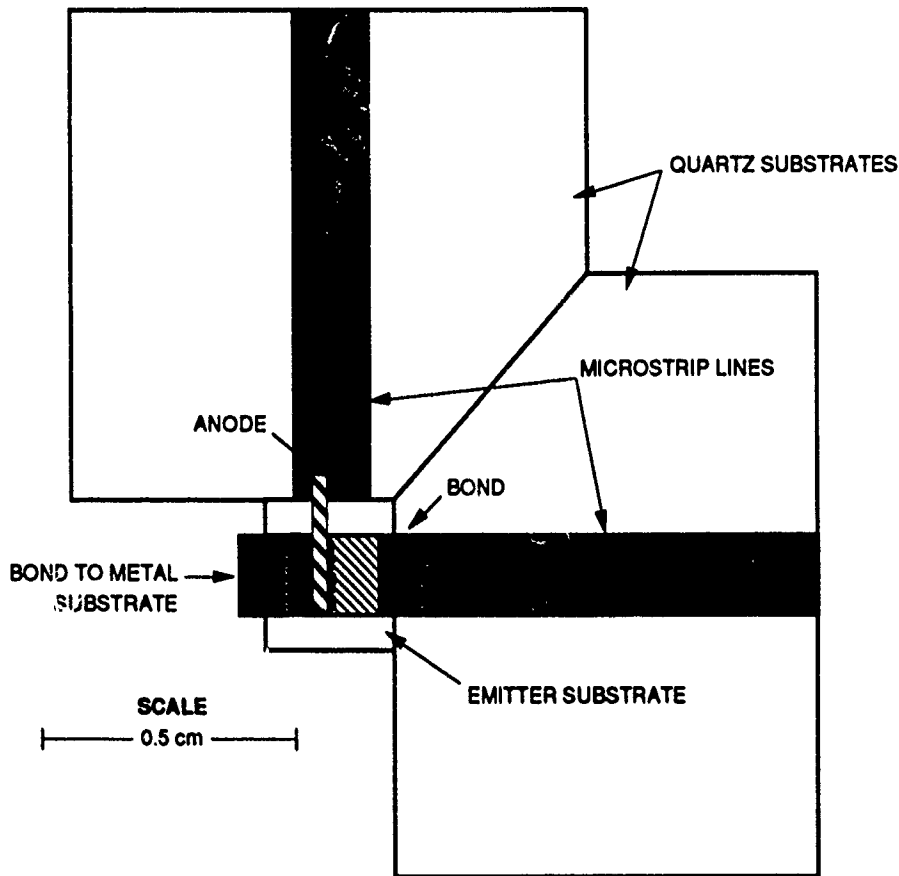
SP-112990-SD

Figure 2. Emitter strip (not to scale)



sp-022992-jd

Figure 3. Top view of emitter strip in Figure 2 on a quartz substrate

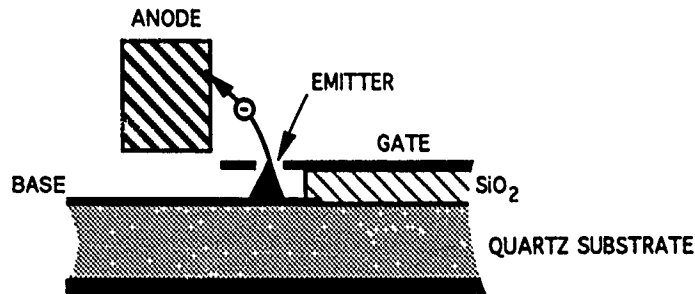


sp-022892-jd

Figure 4. Top view of emitter substrate bonded to two 50-ohm microstrip lines of which one supports the anode

row of emitters. Figure 5 shows a cross-sectional elevation view of the structure as seen from the bottom up of Figure 4. The thicknesses of all three substrates (the two strip lines and the emitter chip) are the same; they will be held in position by a metal ground plate (not shown). The cathode chip is clamped to the ground plate by the base-grounding strap, and the microstrip substrates will be clamped at the edges—well away from the microstrip lines so that the clamps will not be a significant factor in the microwave impedance of the microstrip lines. The cathode chip bonds will be made so that the cathode can be replaced as desired. Everything in Figure 4 is meant to be a permanent fixture except the cathode; thus, many cathodes can be tested for comparison in the same test fixture.

Figure 6 shows the complete test assembly. We will mount coaxial connectors on the ground plate so that their center conductors make contact to the microstrip lines addressing the gate and anode. The connectors will be coupled to coaxial cables that feed the microwave signal through a demountable flange on the vacuum housing that encloses the triode test assembly. Four test fixtures will be mounted within the vacuum housing so that up to four tests can be made with each vacuum pumpdown cycle. (The pumpdown, which includes a 400 to 450°C vacuum bakeout, typically takes about two days.) We will assemble two test vessels so that one can be processed while the other is under test.



sp-02792-jd

Figure 5. Cross-sectional view of the structure in Figure 4 seen from the bottom up

Having to work under ultrahigh vacuum conditions with the required bakeout complicates the design of the test fixture. Ordinary solid-state microwave procedures such as soldering contacts and modifying the circuit during the testing will not be possible. Furthermore, the coaxial cables and connectors must be able to withstand the 400 to 450°C bakeout. Fortunately, semirigid, hermetically sealed, SiO<sub>2</sub>-insulated cables and connectors that meet these requirements are commercially available (Kaman Industries, Colorado Springs, Colorado).

We plan to make the ground contacts to the microstrip lines by using bump bonding, which will be discussed in Section 3 on fabrication.

### 3. LOW-CAPACITANCE CATHODE FABRICATION

Figure 7 is a detailed schematic of the cathode concept shown in Figures 2 and 3. We have designed and fabricated photomasks for patterning the structure shown; studies of fabrication procedures to achieve the desired cathode geometries are in progress. The photolithography has been done with the cooperation of an outside vendor because a sophisticated, specialized, and expensive photolithography stepper is required to achieve the required dimensions and registration. The dielectric deposition is being done by the outside vendor for the same reasons.

As a first step in the fabrication process, the stepper-lithography vendor checked the masks for alignment specifications by using aluminum metal electrodes; they were found to be within specifications. Test structures were then made using our standard electrode material (molybdenum). However, we found that the molybdenum etch normally used for patterning molybdenum undercut the photoresist excessively for this application. This was not particularly surprising, because the overlap area is only 4- $\mu\text{m}$  wide in our preferred configuration and even a very small undercut (e.g., 2  $\mu\text{m}$ ) can be too much. Unfortunately, it was impossible to control the width of the overlap to the desired tolerances using molybdenum, but we have found that using the same photolithographic procedures, we can etch chromium films to very well-defined edges and tolerances with negligible undercutting. Therefore, chromium was used for the base electrode material in fabricating the first test structures. Molybdenum was used for the gate electrode because we have a well-developed process for etching precise holes in molybdenum, and

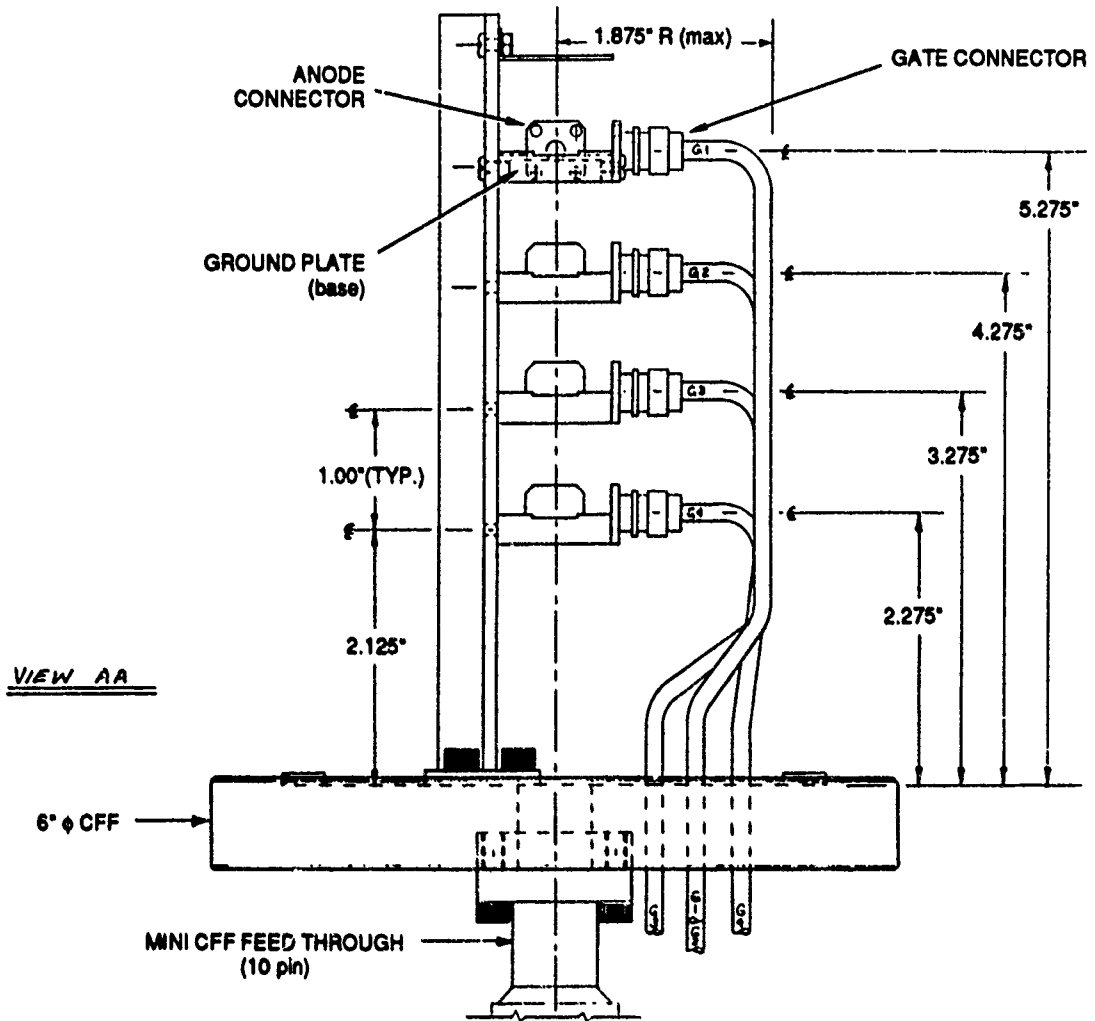


Figure 6. Layout of the high-frequency test apparatus with sites for four cathodes

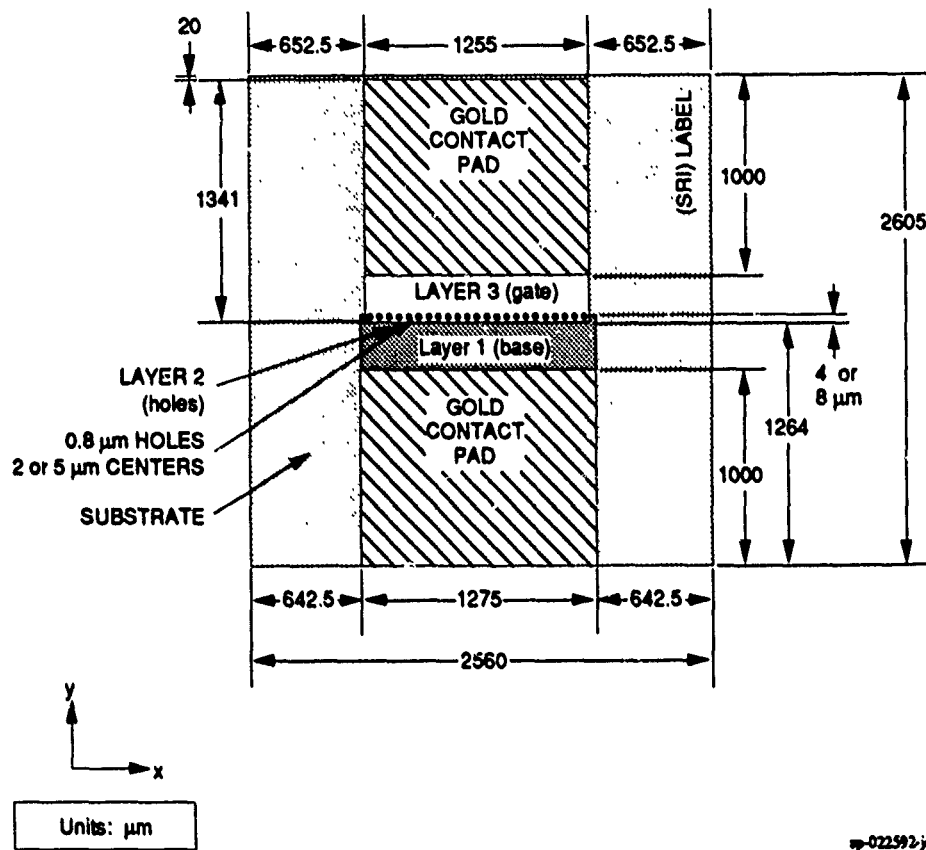


Figure 7. Detailed low-capacitance cathode layout

gate-hole diameter and uniformity are critical issues in cathode performance (the molybdenum hole-etch procedure unfortunately does not lend itself to edge etching).

In this low-capacitance design, the dielectric layer must be a deposited oxide rather than a thermally grown oxide (which we used in the past when working on silicon substrates). The change is not a fundamental problem, since the first cathodes built in this laboratory 25 years ago were formed on sapphire substrates with a deposited (evaporated) aluminum oxide film for the dielectric layer. However, the evaporated oxide is marginal from the point of view of dielectric constant and pinhole density. Since that time, the technology of chemical vapor deposition (CVD) has advanced considerably and is now the preferred process for dielectric deposition. We do not have CVD apparatus capable of handling 5-inch wafers in our laboratory, and we must use 5-inch wafers for this work in order to be compatible with the optical lithography stepper available to us. Therefore, we must have the oxide deposited for us until we have an in-house CVD available to us that can handle 5-inch wafers.

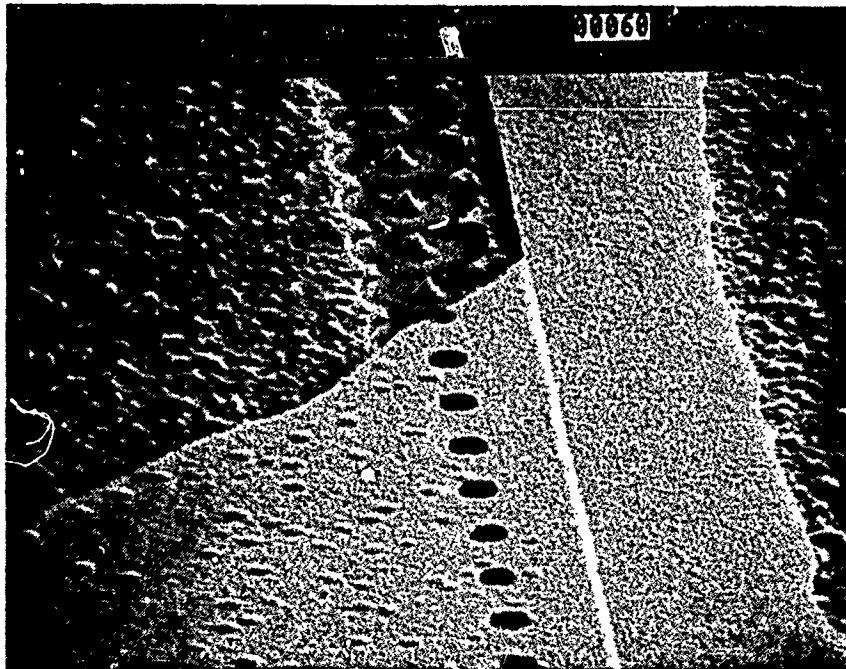
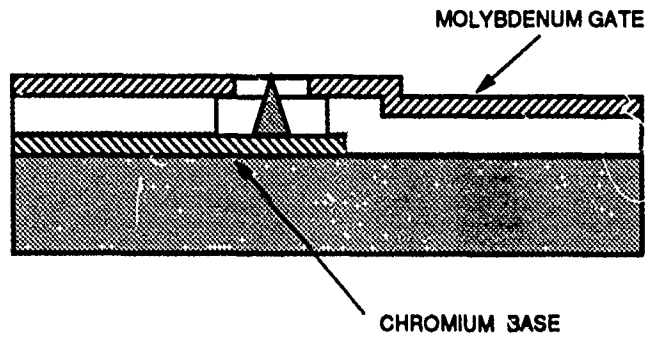
The first tests with depositing the dielectric layer were done with atmospheric pressure CVD (APCVD) phosphorus-silicate glass (PSG) over a patterned chromium-base film. The result was disappointing in that the chromium was severely oxidized during the process. However, adding a thin layer of spin-on glass (SOG) over the chromium prior to the APCVD process was found to prevent oxidation of the chromium during APCVD. We will investigate a variety of other materials, CVD processes, and sputtering techniques in the course of our process development.

As part of the deposition process development, we fabricated structures to test compatibility with the cone formation process. The first test structures for this purpose consisted of a patterned chromium-base film, an APCVD dielectric layer of PSG, and a molybdenum gate film patterned with a row of holes along the edge of the base film as shown in Figure 7. The gate electrode shape is patterned as a last step after the cones are in place. The base and gate films were deposited at SRI, and the APCVD PSG dielectric layer was deposited by the vendor.

The standard molybdenum cone formation process was performed on the structure, and the aluminum/alumina sacrificial parting layer was etched off using one of our standard parting layer etchants, potassium hydroxide (KOH). We used KOH because our usual parting layer etchant, phosphoric acid, attacks chromium which was used as the base film in these structures. (Much of our prior work has been on silicon substrates; there, KOH can be used only briefly, because it attacks silicon rapidly.)

The result of this first cone formation test was disappointing in that the PSG layer did not hold up to the KOH, and the gate film was undercut excessively during the etch-off of the sacrificial layer. This was a surprise, because KOH should not attack PSG so vigorously. Close inspection of the structure showed that the molybdenum gate film did not adequately protect the PSG film because of a roughness of the PSG layer that led to vias in the overlying molybdenum film. The vias are due to poor "step coverage" of the rough features on the PSG surface because of the highly directional nature of the evaporation process used to deposit the molybdenum. We are confident that the excessive roughness of the PSG layer is abnormal and can be greatly improved. It is likely that this first trial PSG deposition was, for some reason, out of specification, leading to poor stoichiometry and surface roughness. The roughness led to pinholes that exposed the PSG to the KOH, and the poor stoichiometry led to the excessive KOH etch rate. Figure 8 shows an electron micrograph and schematic of this low-capacitance structure with the dielectric layer overetched and the gate film broken away from large areas as a result.

Subsequent experiments have produced improved dielectric layers, although some difficulties are still being experienced with breakup of the PSG layer. Nevertheless, some low-capacitance cathode structures have been fabricated that were good enough to attempt electrical tests, and some very encouraging results have been obtained. These are discussed in Section 4. Different metals, dielectric materials (e.g., borophosphosilicate glass or BPSG and  $\text{SiO}_2$ ), and deposition procedures will be investigated during ongoing studies of the fabrication processes. In addition, SRI has obtained a sputtering system capable of depositing metal and dielectric layers on 5-inch wafers, and this will be on-line and available for material studies shortly.



sp-023492-jd

Figure 8. SEM and cross-section of a portion of a low-capacitance cathode structure with the dielectric layer undercut so that the gate film lifted and broke away from a large area

## 4. CATHODE EMISSION TESTS

Cathode emission tests have been carried out in three study areas: (1) how to achieve stable performance with close-spaced anodes, (2) means for lowering the operating voltage requirements, and (3) the performance of the low-capacitance cathode structures now under development.

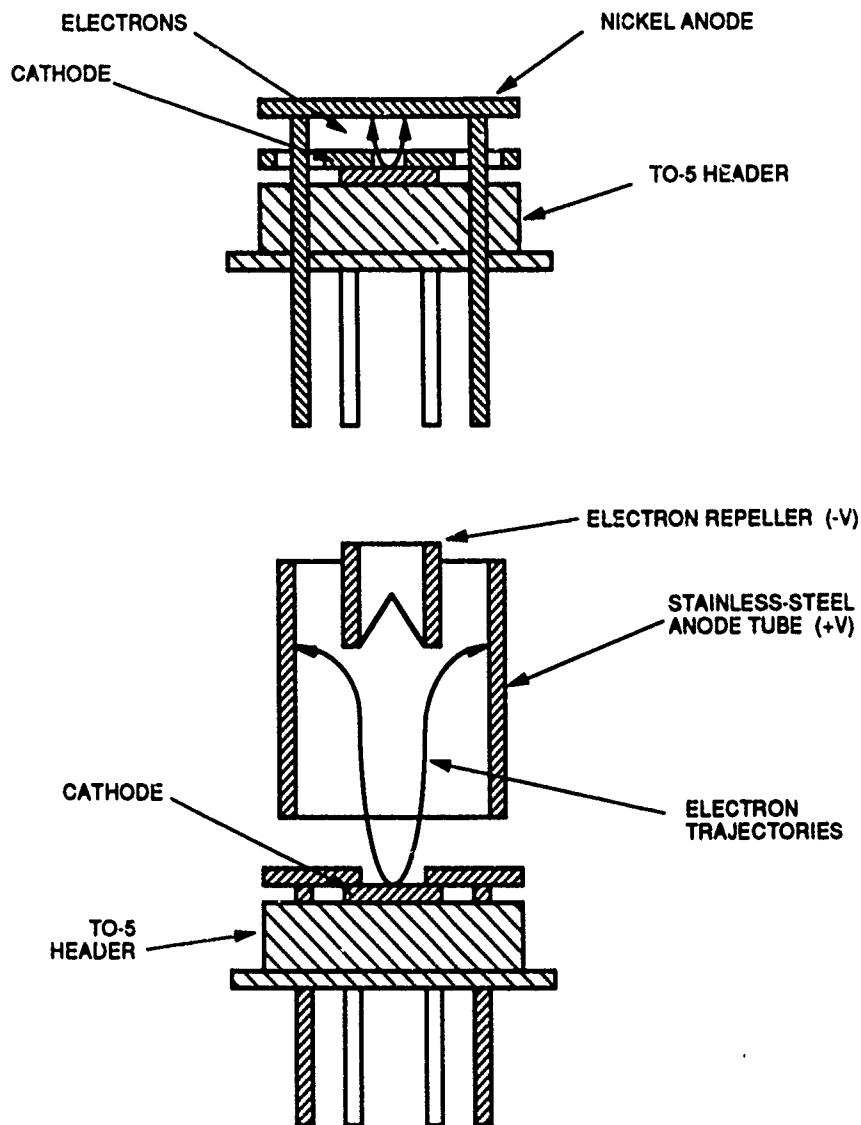
### 4.1 CLOSE-SPACED ANODES

In work done prior to this project, it was shown that the field-emitter arrays are capable of up to at least  $1000 \text{ A/cm}^2$  of emission (Spindt et al., 1991), and that tip loadings of at least  $500 \mu\text{A}/\text{tip}$  are possible (Spindt et al., 1984). In general, our experience with probing these high-performance regimes has shown that limitations on performance are more often associated with power dissipation at the collector than with the ability of the emitter array to produce emission. Having to work with small, close-spaced anodes can be a severe problem with regard to power handling, outgassing, and arcover, unless the anodes are of the proper material and very carefully processed.

In an effort to learn more about the effects of close-spaced collectors, collector materials, and collector processing on the performance of the emitter arrays, we mounted three cathodes having 1000 tips in an area  $256 \times 256 \text{ }\mu\text{m}$  square (packing density of  $1.5 \times 10^6 \text{ tips/cm}^2$ ) in each of two test vessels. One test vessel was used as a control and was fitted with our often-used 3/8-inch-diameter 304 stainless-steel tube anodes and mounted about 3 mm from the cathodes so that the electron beam was emitted down the bore of the tube. The second test vessel was equipped with small nickel-plate anodes mounted on the TO-5 header with the cathodes. The nickel-plate anodes are parallel to the cathode chips and about 1 mm from the cathodes. The two types are shown in Figure 9. In each case, the anodes were pretreated in the same way that the anodes used in our traditional test systems are prepared: the anodes were chemically cleaned, hydrogen fired at 1400K for one-half hour, and then heated in vacuum by electron bombardment until all evidence of outgassing disappeared.

The vessel with stainless-steel tube anodes was capable of handling more power than the TO-5-mounted nickel-plate anodes because of the larger area of the tube-shaped anode. In addition, the close spacing between the TO-5-mounted nickel-plate anode and the cathode ( $\approx 1 \text{ mm}$ ) increases the power density to the nickel-plate anode because the electron beam doesn't have space to spread out before impacting the anode. Pumpout of any gas evolved from the nickel-plate anode was also restricted by the close spacing.

After pumpdown and bakeout, the emission level was brought up to 10 mA from each cathode with nickel-plate anodes using a 60-Hz half-wave driving voltage (20% duty cycle) and 180 V on the anode. The cathodes in the test vehicle with the stainless-steel anodes were also slowly increased in emission up to 10 mA with the 60-Hz half-wave drive, but with 600 V on the



sp-022692-jd

Figure 9. Schematic cross-sections of the close-spaced integrated nickel-plate anode and the stainless-steel tube anode

anodes. A higher voltage was necessary with the tube-type anode because the geometry of the tube configuration produces a lower electric field at the cathode surface, and space charge effects cause emitted electrons to return to the gate if the field is insufficient.

The cathodes were left operating at these levels for several days. Under these conditions, the emission slowly increased, and the voltage had to be reduced to prevent excessive emission and overheating of the anodes. Nevertheless, the emission from the cathodes in the system with the stainless-steel anodes climbed to 20 mA while the cathodes were unattended for a short time and overheated the anodes. This is not common, but has happened before. As a result of the

excessive heating of the anodes, an electrical leakage developed between the base and gate films of all three cathodes in the stainless-steel anode system. It is not clear at this time whether the leakage was due to evaporation of material from the stainless steel onto the cathodes, overheating of the cathodes, overheating of the TO-5 cathode mounts, or some combination of these possibilities. During subsequent operation, the leakage continued to increase, and the voltage required to maintain emission also increased slowly with time. Eventually, one of these cathodes failed to a short circuit. The other two cathodes were then held at 10 mA peak emission and shown to be stable at that level for 4 weeks, at which time they were shut down. Figure 10 is a plot of the emission current vs. the reciprocal of the applied voltage for the remaining two cathodes (53i-300-8Q and 53i-300-8T) in the stainless-steel-anode vessel just prior to shutdown.

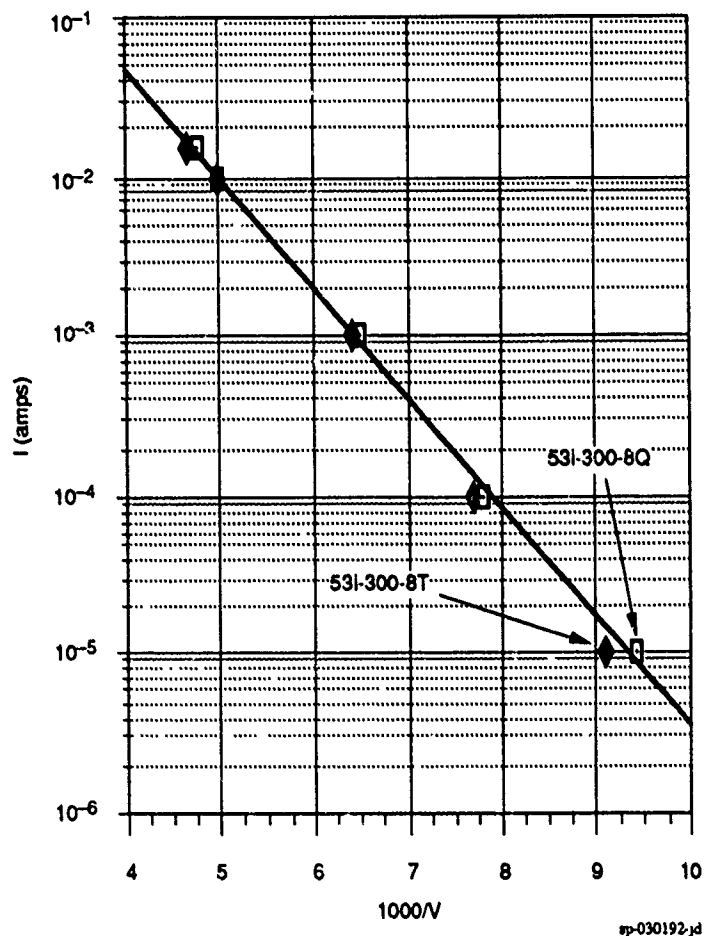


Figure 10. Emission data for 53i-300-8Q and 53i-300-8T (1000 emitter tips)

An important point to make is that the results described above are essentially identical to those obtained in an earlier experiment with the same apparatus except that 10,000-tip arrays were used. It seems clear that the performance limits are due to anode loading rather than cathode loading, and that the cathodes may well be capable of much higher performance than we usually observe because of power dissipation limitations with the collectors in most of the test set-ups.

The cathodes in the system with the nickel-plate anodes have operated well up to 15 mA peak emission (15  $\mu$ A/tip). During this time, the emitters slowly improved with regard to the voltage required to maintain a given emission. They have not been pushed beyond 15 mA because space charge effects caused the gate current to become higher than we like ( $\approx$  0.5 mA). We are limited in the voltage that can be applied to a collector that is mounted on the TO-5 header. In addition, the nickel-plate anodes were obviously getting very hot and, in view of our experience with the stainless-steel collectors, we decided to maintain emission at 15 mA and observe the long-term effects of the close-spaced nickel-plate anode on the cathode's performance. At the end of one week, two of the cathodes in the nickel-plate anode system were stable but, oddly, the third degraded over several days and finally failed to a short. All three cathodes were from the same substrate, were processed together, were mounted in the same chamber, and were driven in the same way for the same time. The reason for the difference in the behavior of the one cathode is not clear at this time. The other two cathodes were shut off due to a power outage just before the Christmas holiday. After the 10-day holiday recess, the remaining two cathodes were again brought up to 15 mA with 180 V on the collectors and have been operating at that level since the beginning of January. Figure 11 is a plot of the emission current vs. the reciprocal of the applied voltage for the data from one of the cathodes (53i+300-7P) taken at the beginning of the test and after several months of operation. The second remaining cathode (53i+300-7Q) is essentially identical. The performance shown in Figure 11 is considerably better than that obtained with the stainless-steel control cathodes shown in Figure 10. This improvement is partly due to cathode shape; the cathodes in the nickel-plate system have relatively tall, sharp tips. In addition, we were very fortunate in getting the close-spaced anode right on our second try (the first was a stainless-steel plate and failed badly). At this point, enough time has been accumulated on the cathodes to make it reasonable to continue their operation as a life test, and we will do so for at least a few more weeks.

From these experiments, we conclude that electronic-grade nickel processed in the way described above prior to mounting with the cathodes appears to be a good candidate for use as a close-spaced anode in a field-emitter array-triode configuration. Power dissipation at the anode appears to be the critical issue limiting cathode performance because excessive heat and out-gassing lead to electrical breakdown.

#### 4.2 LOW-VOLTAGE CATHODE GEOMETRY

In general, it is desirable to have the lowest possible voltage requirements for driving the cathode arrays for reasons of driving electronics, beam optics, energy stored in the cathode base to gate capacitance, losses associated with displacement currents, and maximum  $g_m$ . The most fruitful way to minimize the voltage is to make the gate aperture as small as possible, and to make the emitter tip as sharp as possible, and to position the tip so that it is slightly above the gate film. Fortunately, the emitter-cone formation process is very flexible; we can tailor the shape of the emitter cone by controlling the deposition parameters during the cone formation process. Figure 12 shows a plot of current vs. 1/voltage for two emitter arrays with different gate and emitter geometries but with the same number of emitter tips (1000). Both cathodes have 1- $\mu$ m gate aperture diameters, but in the case of 53i-300-25B, the tips are 2000 $\text{\AA}$  below the bottom edge of the gate film and, while the tips are 4500 $\text{\AA}$  above the bottom edge of the gate film in the case of 53i+300-26B. (The gate film is 2500 $\text{\AA}$  thick in both cases.) The tips are similar in

appearance and are about  $250\text{\AA}$  in radius; however, there may be differences that are too small to measure accurately with the SEM available to us. What is important is that Figure 12 shows that much can be gained by using tall, sharp tips (approximately three orders of magnitude in current emission at 100 V in the example shown).

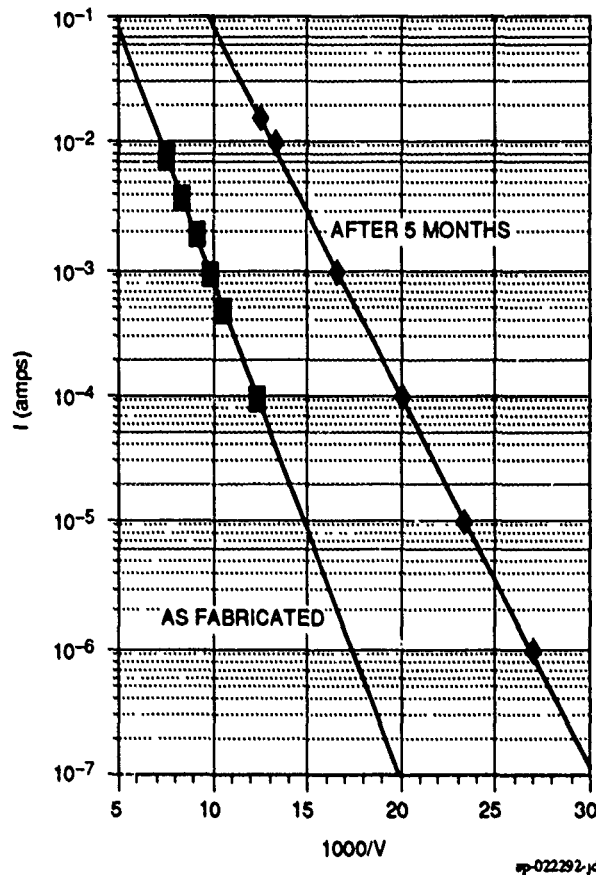


Figure 11. Cathode 53i+300-7P as fabricated and after 5 months (3600 h) of operation (1000 emitter tips)

#### 4.3 EMISSION TESTS WITH LOW-CAPACITANCE CATHODES

The first cathodes fabricated in the low capacitance configuration shown in Figure 2 have been tested. Although more work remains to be done on the dielectric-layer deposition, one of the cathodes performed very well—especially in view of the fact that the emitter tips were relatively short and blunt. The cathode (100L-A5-1A) was of the type having a  $4\text{-}\mu\text{m}$  overlap of the base and gate electrodes and a tip-to-tip spacing of  $2\text{ }\mu\text{m}$ . Thus, the total number of tips is 625 in a single 1.25-mm line. The cathode was driven with a square-wave pulse at a low (5%) duty cycle to prevent overheating of the collector. Figure 13 shows oscillographs of the output current pulse and the modulating signal added to the gate while the cathode was turned on by the driving voltage pulse. The emission current pulse is 5 mA per major division, and the modulation signal is 5 V per major division. At the 25-mA emission level shown, the transconductance is  $500\text{ }\mu\text{S}$  or  $0.8\text{ }\mu\text{S}$  per tip. We would like this to be higher, and we expect that it will be significantly improved by the more desirable emitter-tip geometry that we are developing.

The gate was modulated during the test at a maximum of 20 MHz, which was the limit of the function generator available to us at this time. The cathode capacitance is about 0.1 pf, and it should be possible to achieve 1-GHz modulation with this kind of structure, especially if the

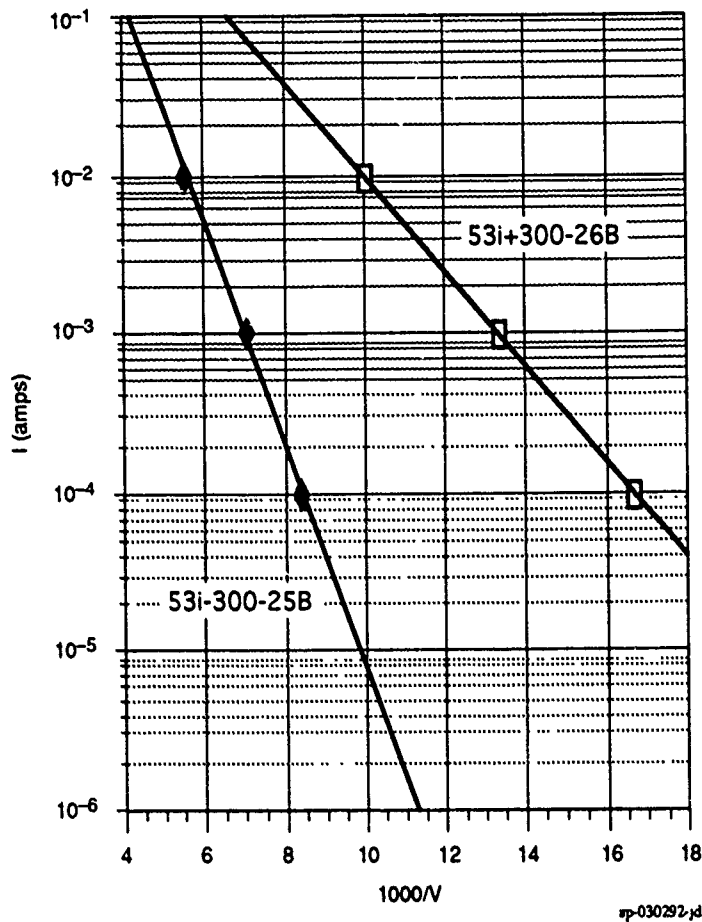


Figure 12. Emission data for 1000-tip cathodes 53i-300-25B (average tips) and 53i-300-26B (tall, sharp tips)

voltage requirement is reduced by improving the gate aperture and tip geometry, both of which can certainly be done. The transconductance,  $g_m$ , required to achieve a given cutoff frequency,  $f_t$ , is  $g_m = 2\pi f_t C_g$  where  $C_g$  is the cathode capacitance ( $\approx 0.1$  pf). At an  $f_t$  of 1 GHz  $g_m$  must be at least 628  $\mu s$ .

Assuming the 1.25-mm-long active area to be 2  $\mu m$  wide (same as the tip-to-tip spacing), the emitting area for the cathode is  $2.5 \times 10^{-5} \text{ cm}^2$ . With the cathode operating at 25 mA, this works out to be a current density of 1000 A/cm<sup>2</sup> averaged over the area occupied by the cathode array. Cathode 100L-A5-1A was operated at this level for two days without change. It was then shut off for a planned SRI-wide power outage over the Christmas holiday. Figure 14 is a plot of current vs. 1/voltage for Cathode 100L-A5-1A at the end of the two days of operation at 1000 A/cm<sup>2</sup>.

Although this first test was very encouraging, further tests of the low-capacitance cathode structures will be put off until better dielectric layers are obtained. We will also fabricate subse-

quent low-capacitance cathode arrays with more desirable emitter geometries in order to reduce the operating voltage.

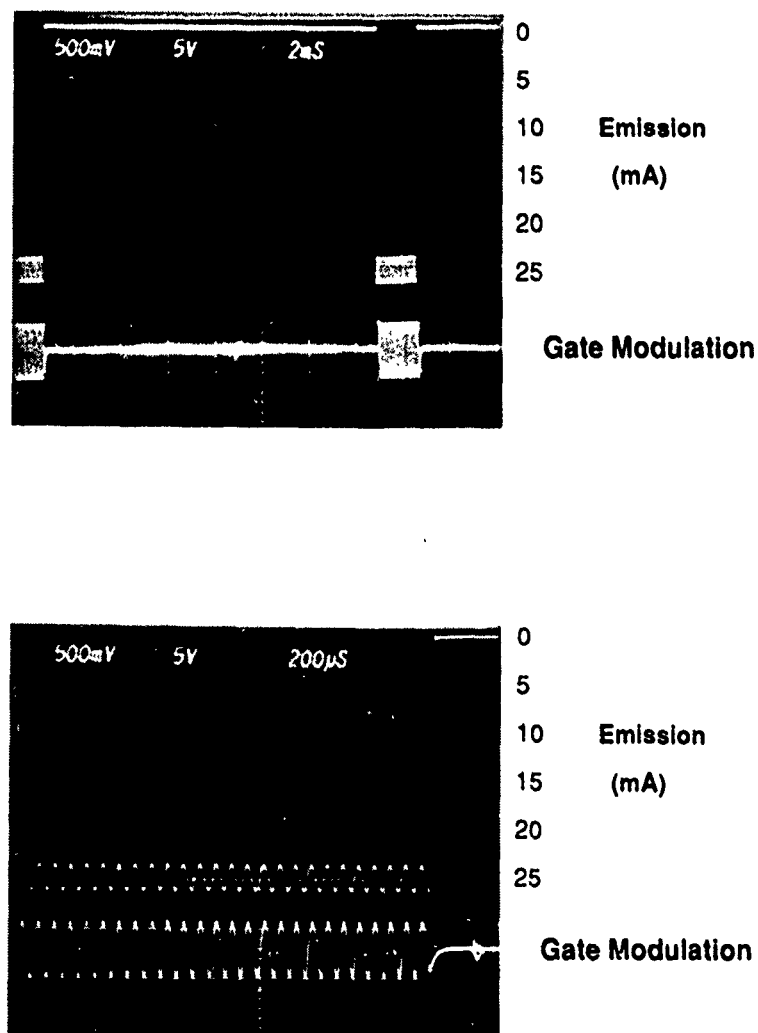


Figure 13. Oscillographs of cathode 100L-A5-1A at 25 mA emission ( $1000 \text{ A/cm}^2$ ) with a 6 V peak-to-peak modulation voltage on the gate electrode. Load resistor =  $100 \Omega$ . Anode voltage = 600 V.

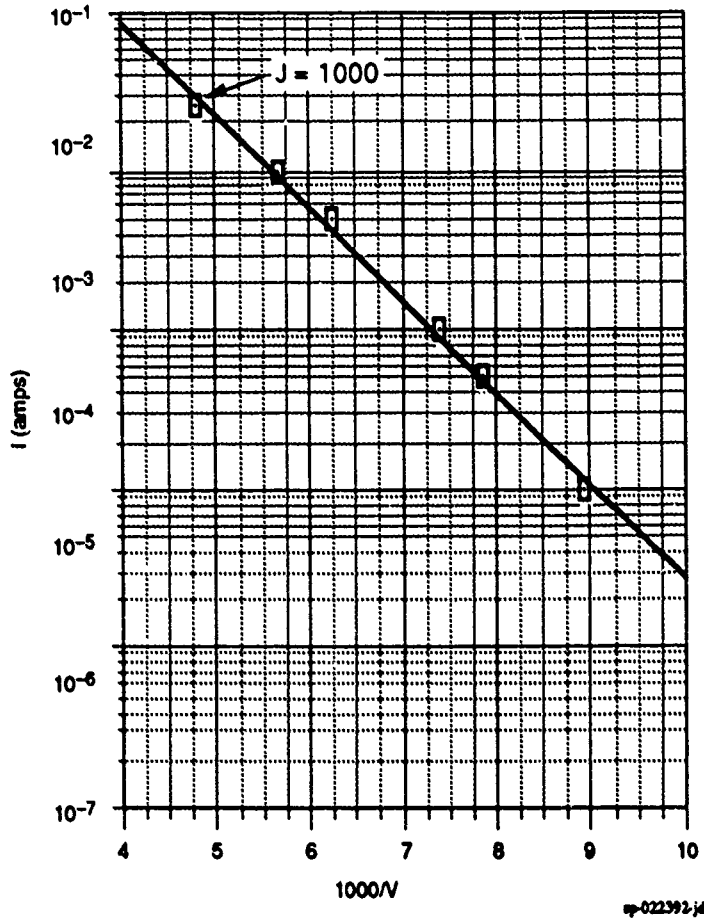


Figure 14. Current vs. 1/voltage plot for low-capacitance cathode 100L-A5-1A up to 1000 A/cm<sup>2</sup>

## 5. MICROWAVE MEASUREMENTS

Active microwave devices, such as FETs and bipolar semiconductors, are usually characterized by measuring their S-parameters which provide a complete picture of their potential performance in all microwave applications. Although the present contract calls only for a demonstration of the ability to *modulate* emission at 1 GHz, it is necessary to measure the S-parameters of the device in order to eliminate all ambiguities. The test fixture shown in Figure 6 was designed for this purpose.

Working at 1 GHz requires that the emitter be operated at a current sufficiently high to provide a significant transconductance. Because this will require working at a high current density (estimated to be a few hundred amps/cm<sup>2</sup>) and an emitter-anode voltage in the range of 100 to 200 V to overcome space-charge effects, power densities to be dealt with at the anode will be rather large (in the 50 W/cm<sup>2</sup> range). So much power would require a heat-sink at the anode,

which would be a troublesome complication at this stage of development. An alternative is to use pulsed measurements to explore the high-performance region; this is what will be done for these first experiments. The measurements will be performed with the HP 8510B network analyzer which allows pulsed microwave measurements (Hewlett-Packard, 1988). At present, we are testing the pulsed measurement procedures on known microwave elements.

Characterizing devices on the network analyzer requires calibration measurements that remove the effects of the coupling fixtures and the network analyzer itself on the measurements. For the purposes of calibration, three calibration fixtures will be needed for the standard so-called Thru-Reflect-Line (TRL) calibration used for noncoaxial measurements (Hewlett-Packard, 1987). The calibration fixtures will be similar to those discussed in connection with Figure 4. For the "thru" measurement, the two microstrip lines will be lined up and connected together. The "reflect" measurement requires a short-circuit at the end of the two lines; the "line" measurement is identical to the "thru" measurement but with a quarter-wavelength-long line added to the connected lines. When all the S-parameters have been measured, we can easily evaluate the use of the triode as, for example, an amplifier. The general expression for the transducer gain,  $G_T$ , i.e., the ratio of the power delivered to the load and the power available from the source, is given by

$$G_T = \frac{|S_{21}|^2 (1 - |\Gamma_S|^2) (1 - |\Gamma_L|^2)}{|(1 - S_{11} \Gamma_S)(1 - S_{22} \Gamma_L) - S_{21} S_{12} \Gamma_L \Gamma_S|^2} \quad (1)$$

where  $\Gamma_S$  and  $\Gamma_L$  are the reflection coefficients at the source and load respectively. The general expression for the reflection coefficient is

$$\Gamma_i = \frac{Z_i - Z_0}{Z_i + Z_0} \quad (2)$$

where  $Z_0$  is usually the 50-ohm line impedance and  $Z_i$  the impedance at port  $i$ . In the simpler case where the power reflected back from the load to the input given by  $|S_{12}|^2$  is zero,  $G_T$  simplifies to the unilateral transducer gain given by

$$G_{TU} = \frac{1 - |\Gamma_S|^2}{1 - S_{11} |\Gamma_S|^2} \times |S_{21}|^2 \times \frac{1 - |\Gamma_L|^2}{1 - S_{22} |\Gamma_L|^2} \quad (3)$$

$G_{TU}$  thus consists of the product of three factors: the first presents the effect of impedance mismatch at the input; the last presents a similar mismatch at the output; and the second,  $|S_{21}|^2$ , is the power gain of the active device provided through its transconductance. Entering the experimental values in these equations will clearly show which factors limit the gain and what can be done to reduce their effect. Matching at the input and output ( $\Gamma_S = S_{11}^*$ ,  $\Gamma_L = S_{22}^*$ ) maximizes the gain to

$$(G_{TU})_{\max} = \frac{|S_{21}|^2}{(1 - |S_{11}|^2)(1 - |S_{22}|^2)} \quad (4)$$

For absolute stability of the amplifier with a passive source and load impedance, the following conditions must be met

$$|S_{11}| < 1, |S_{22}| < 1 \quad (5a)$$

$$\left| \frac{|S_{12} S_{21}| - |M^*|}{|S_{11}|^2 - |D|^2} \right| > 1 \quad (5b)$$

$$\left| \frac{|S_{12} S_{21}| - |N^*|}{|S_{22}|^2 - |D|^2} \right| > 1 \quad (5c)$$

where

$$D = S_{11} S_{22} - S_{12} S_{21} \quad (6a)$$

$$M = S_{22} - D S_{22}^* \quad (6b)$$

$$N = S_{22} - D S_{11}^* \quad (6c)$$

## 6. WORK PLANNED

During the next period, we will begin fabrication of the microwave test vehicle and continue the development of the low-capacitance cathode structure. In addition, we will continue to study methods to further reduce the voltage requirements for emission.

## REFERENCES

- Holland, C.E., A. Rosengreen, and C.A. Spindt, 1991: "A Study of Field Emission Microtriodes," *IEEE Trans. Elec. Dev.* 38(10), October.
- Hewlett-Packard, 1988: HP 8510B Network Analyzer: "Introductory Pulsed RF-Measurements User's Guide," HP Part No. 08810-90183, Hewlett Packard, December.
- Hewlett-Packard, 1987: "Applying the HP 8510B TRL Calibration for Non-Coaxial Measurements," HP Product Note 8510-8, Hewlett Packard, October.
- Hewlett-Packard, 1968: "S-Parameters...Circuit Analysis and Design," HP Applications Note 95, Hewlett Packard, 3-12, September.

Spindt, C. A., C.E. Holland, and R.D. Stowell, 1984: "Recent progress in low-voltage field-emission cathode development," *J. de Phys. Comp.* C9, Supp. to Vol. 45, No. 12, 269, December.

Spindt, C. A., C.E. Holland, A. Rosengreen, and I. Brodie, 1991: "Field-emitter arrays for vacuum microelectronics," *IEEE Trans. on Elec. Devices* 38(10), October.